Book of Tutorials and Abstracts

European Microbeam Analysis Society

EMAS 2024

14th
REGIONAL WORKSHOP

on

THE EDGE OF NEW EM AND MICROANALYSIS TECHNOLOGY

12 to 15 May 2024
at the
Brno University of Technology, Brno, Czech Republic

Organised in collaboration with:
Brno University of Technology (VUT)
Central European Institute of Technology (CEITEC)

EMAS
European Microbeam Analysis Society eV
www.microbeamanalysis.eu/

This volume is published by:
European Microbeam Analysis Society eV (EMAS)
EMAS Secretariat
c/o Eidgenössische Technische Hochschule, Institut für Geochemie und Petrologie
Clausiusstrasse 25
8092 Zürich
Switzerland

ISBN 978 90 8227 6978
NUR code: 971 – Materials Science

EXTENDING EBSD CAPABILITIES USING DIRECT DETECTION AND SPHERICAL INDEXING

René de Kloe

Ametek BV, EDAX/Gatan
Ringbaan Noord 103, 5046 AA Tilburg, The Netherlands
e-mail: rene.de.kloe@ametek.com

René de Kloe studied geology at Utrecht University in The Netherlands with structural geology and materials science as main subjects. During his MSc thesis on "Deformation and pressure indicators in natural fault rocks from New Zealand" and later during his PhD thesis on "Nanometre scale melt microstructures in experimentally deformed upper mantle rocks", he worked extensively with both scanning and transmission electron microscopes. During his research he started using EBSD and after obtaining his PhD in 2001, he had the opportunity to join EDAX as applications specialist for EBSD and later also EDS at EDAX in Tilburg, The Netherlands. In this position, his focus is on instrument demonstrations, conference and workshop presentations, and customer support. This includes (on-site) training courses, assistance with analytical problems, and scientific collaborations. Although focussed on Europe, his work has brought him to customers and conferences all over the world.

1. INTRODUCTION

Electron backscatter diffraction (EBSD) is a SEM-based technique to measure and characterise the microstructure of crystalline materials. EBSD is based on capturing the diffracted electron signal from a steeply tilted sample in which the crystal lattice is accessible at the surface of the sample. From the diffraction patterns, the phase and/or crystal orientation of the grain in the sample surface may be determined. For successful analysis, the sample must be crystalline with the crystal lattice extending to the surface of the sample. Some manufacturing techniques directly produce a crystalline surface (e.g., deposition) and do not need additional polishing, but more commonly, the analysis surface needs to be prepared by sectioning and subsequent polishing of the sample to remove all distortion and contamination from the surface. This polishing step is crucial as the information depth for the EBSD patterns is typically less than 50 nm.

EBSD patterns are generated in a 2-stage scattering process (Fig. 1). When the primary beam enters the crystal, the electrons scatter inelastically in all directions, thereby forming the full electron interaction volume that for example produces the EDS signal. The point of initial scattering can be described as a virtual point source that is located at 10 - 50 nm below the surface depending on the material. Electrons that scatter towards the surface of the tilted sample may now elastically diffract on the crystal lattice planes and create an EBSD pattern.

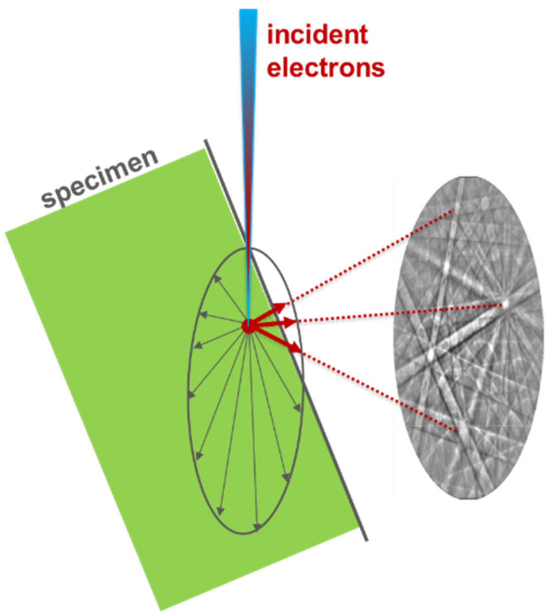

Figure 1. Source volume of EBSD pattern.

The detection of the patterns is done using a specialised detector mounted on the side of the SEM chamber and which can be inserted to a position of ~2 cm from the specimen. In the conventional configuration, an EBSD detector uses a phosphorescent screen on the front to convert the captured electron signal into light, which is then transferred to a sensitive CCD or CMOS sensor inside the detector body (Fig. 2). The resulting image is processed and filtered to isolate the diffracted electrons carrying the crystallographic orientation information from the backscatter signal from the sample surface. This method has been used since the introduction of automated EBSD mapping in the early 1990's. Continuous development of these detectors has improved data collection speeds from ~0.25 pps to more than 6500 pps in the latest EBSD systems.

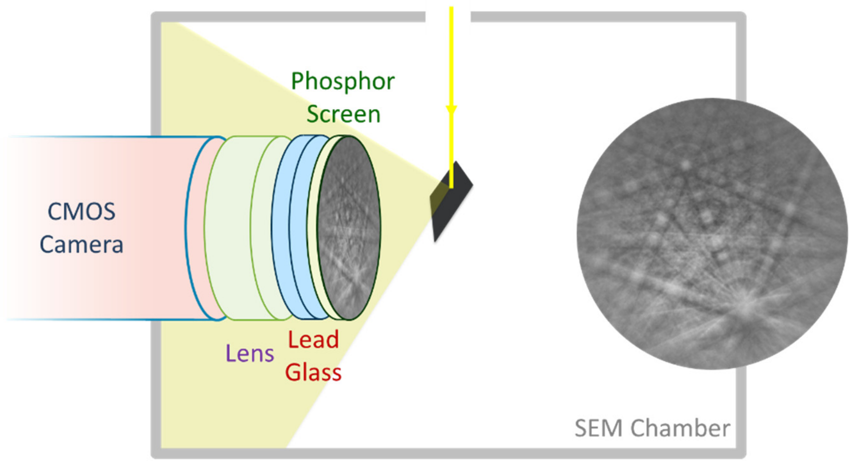

Figure 2. EBSD detector geometry.

2. *DIRECT DETECTION*

Drawbacks of the imaging chain used in conventional EBSD detectors are a loss of efficiency in the electron-to-light conversion at lower electron energies and a certain amount of blurring of the diffraction patterns in the phosphorescent screen and the optics behind it. This limits the obtainable details in the diffraction patterns and EBSD data collection on extremely fine-grained or beam sensitive materials (Figs. 3 and 4). These limitations can be overcome by eliminating the phosphorescent screen and thus the conversion of electrons into light by detecting the (diffracted) electrons directly.

The direct detector is located in the conventional EBSD geometry and electrons are captured using a hybrid-pixel detector with a silicon top sensor bonded to multiple readout chips. When an electron hits the sensor, electron-hole pairs are created. The bias voltage applied across the sensor then pulls the signal to the underlying chip where it is amplified, thresholded, and counted. This way, single event detection is possible and electrons with energies down to 3 kV can be observed (Fig. 5).

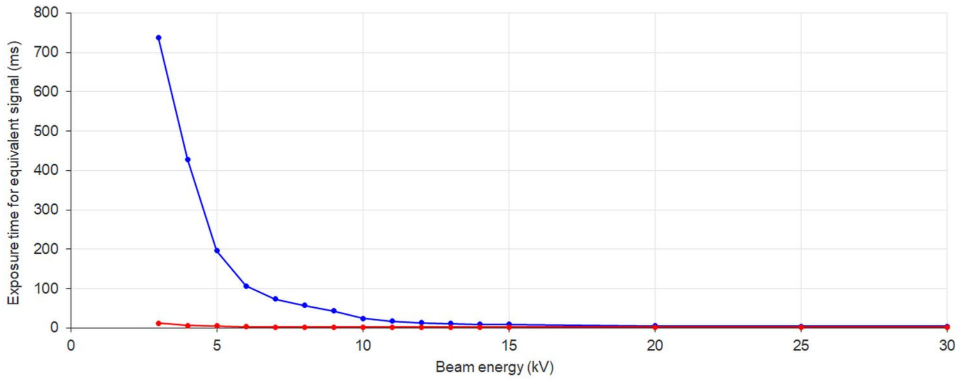

Figure 3. Detector sensitivity versus beam energy; Red: direct detection, Blue: conventional detector.

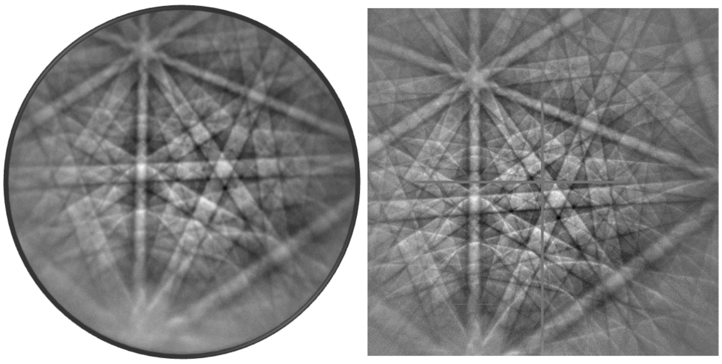

Figure 4. EBSD pattern collected with conventional detector (left) and direct detector (right). Sample and beam conditions are identical.

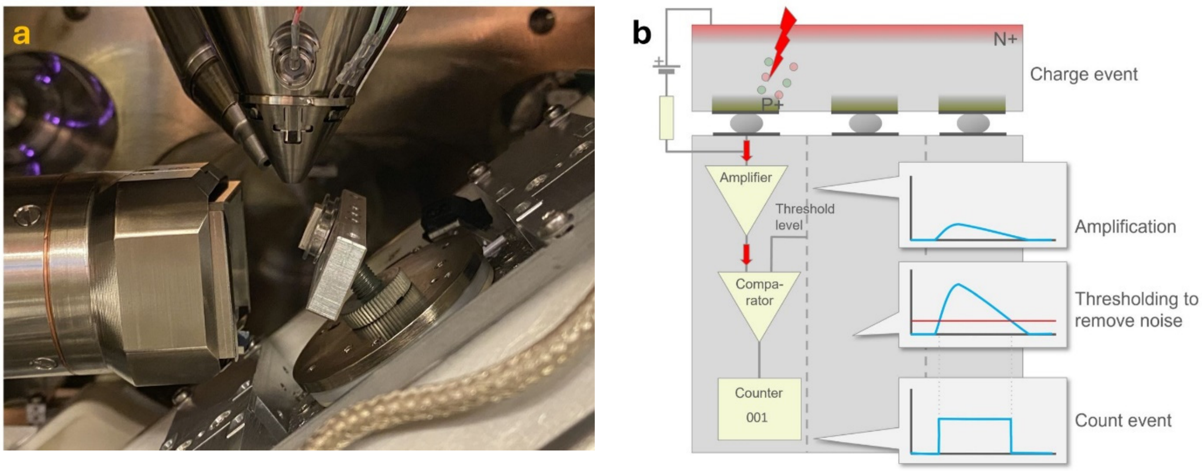

Figure 5. a) Direct detector in standard EBSD geometry in the SEM chamber. b) Signal processing in the direct detector.

With the noise level in the electronics below the 3 kV threshold, it is ensured that only the electron signal coming from the sample is captured and any system noise is avoided. This is critical as in most materials only 5 - 15 % of the electrons that reach the detector have actually diffracted in the crystal lattice and 85 - 95 % of the electrons are backscattered without any orientation information. Considering the ratio of diffracted electrons over backscattered electrons, the lower limit of required electron signal for indexable patterns is ~10 electrons per pixel (Figs. 6a and 6b). Effectively, bands with an excess intensity of 1 electron per pixel over the background can thus be detected. When higher electron intensities are used, highly detailed patterns can be obtained and used to investigate crystallographic details (Fig. 6c).

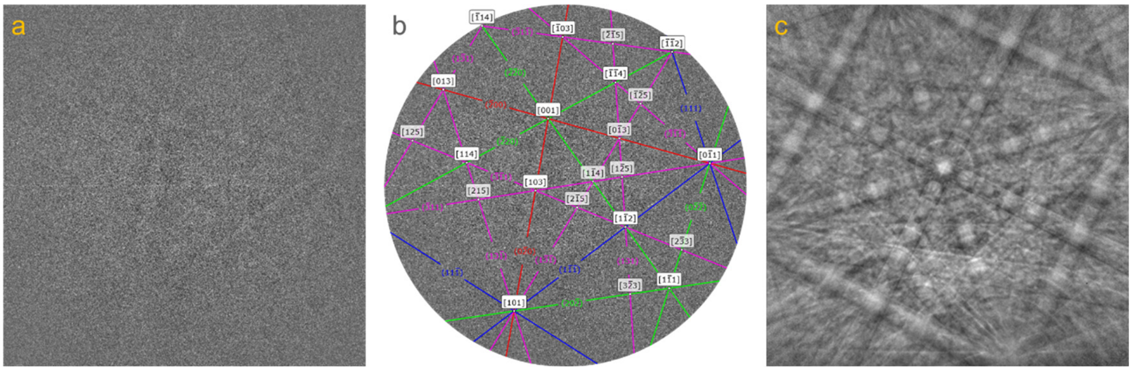

Figure 6. Direct detector EBSD patterns: a) Minimum electron intensity (average 10 electrons/pixel); b) With indexing result; c) Direct detector pattern of $Cr_{23}C_6$ with maximum signal (~11,500 grey levels).

The low noise also allows collection of pattern details in high resolution using a variable sample-to-detector distance, which is impossible on conventional detectors as the signal to noise ratio decreases with sample to detector distance (Fig. 7).

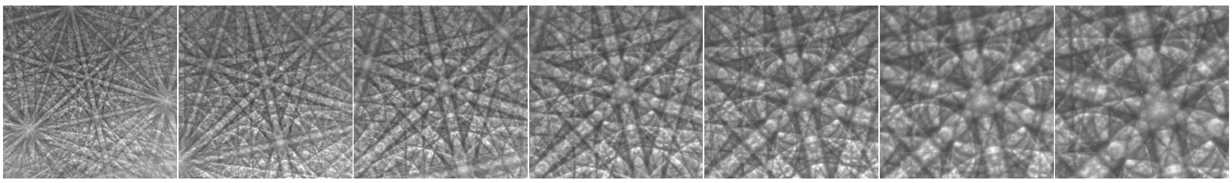

Figure 7. Sequence of Pt patterns collected by retracting the detector in 10 mm steps from 25 to 85 mm detector to sample distance.

The enhanced sharpness can be illustrated by creating intensity profiles across identical bands collected using the two types of detectors. The overlay highlights the blurring effect of the phosphor/optical path, which exceeds the pixel size on the patterns (Fig. 8).

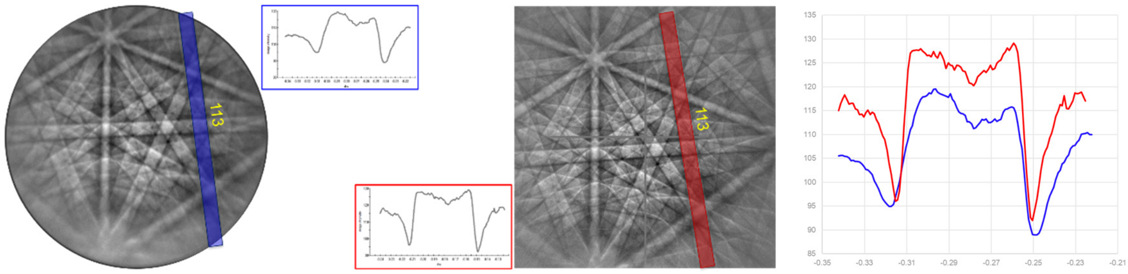

Figure 8. Intensity profiles of a (113) band in EBSD patterns collected on a conventional detector (blue) and a direct detector (red).

3. *LOW DOSE EBSD MAPPING*

Beam sensitive materials such as biological samples containing organic structures, or photovoltaic perovskites with carbon-based structures, deteriorate under the beam dose of conventional EBSD analysis. Low-dose EBSD with 10 - 200 pA beam currents and energies below 10 kV is required for the analysis of such materials. The high sensitivity of direct detection also enables improved lateral resolution in EBSD maps by the reduction of the diameter of the electron beam when using lower beam currents (Figs. 9 and 10).

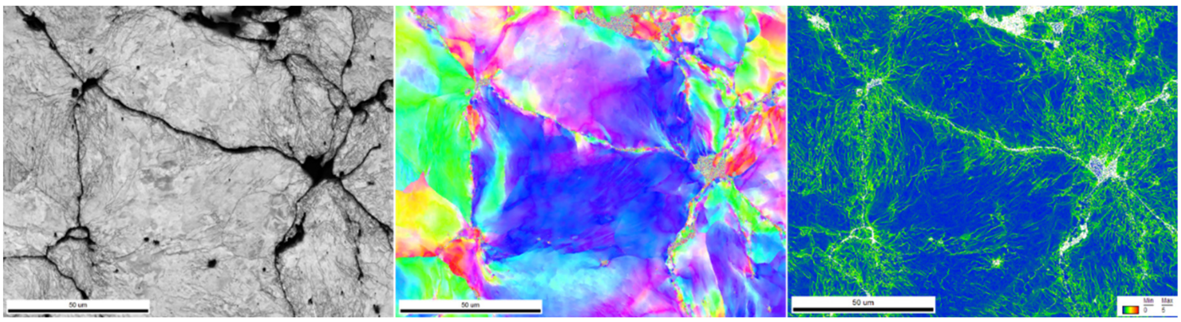

Figure 9. Direct detector EBSD map on cold pressed ferrite powder sample collected using 200 pA beam current.

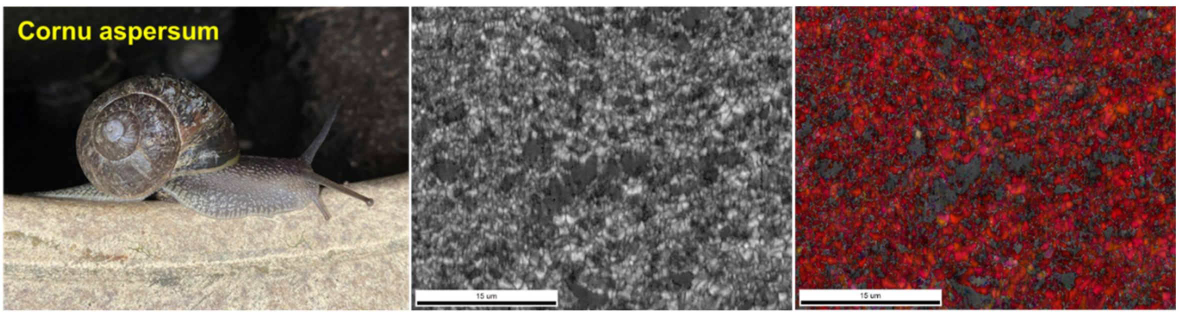

Figure 10. Direct detection EBSD mapping on the shell of a common garden snail. The surface contains both organic and carbonate areas and is measured in native state without any specimen preparation.

Note that the lateral resolution that may be obtained in EBSD mapping is mainly a function of the density of the material and the effective beam diameter. EBSD maps are typically collected with beam currents of 5 - 10 nA and the corresponding beam diameter will then slightly blur edges and grain boundaries. Using beam currents from 20 - 800 pA will improve the sharpness and detail visible in EBSD maps and applies to any material. The primary beam energy has a limited effect on the lateral resolution and mainly affects the depth of the virtual point source, which only becomes visible at step sizes smaller than ~100 nm.

4. ORIENTATION DETERMINATION

After the patterns are detected, the orientation needs to be determined. The conventional method is to detect the bands using the Hough transformation and then match the detected bands against a structure file or lookup table which contains the crystallographic information of the phase being investigated (Fig. 11).

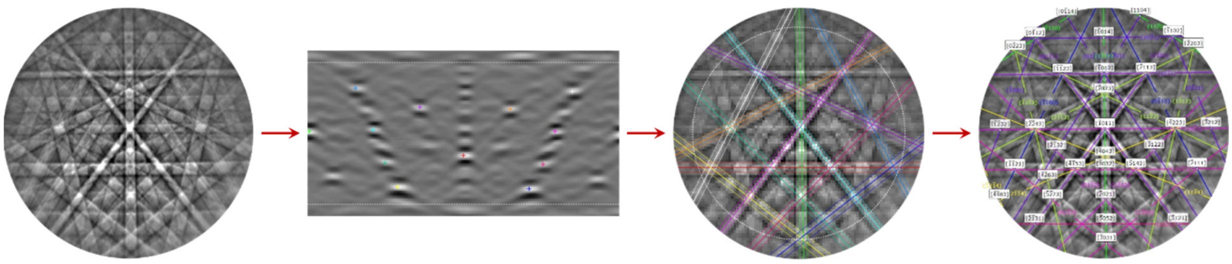

Figure 11. Hough indexing workflow: Detected pattern is converted into Hough transform, bands are detected, and orientation is determined.

This method is highly efficient for fast band detection and indexing, but there are a few requirements to the EBSD patterns to get consistent and reliable indexing and orientation determination:

- Consistent band detection
  - *Actual bands need to be detected, no artefacts.*
- Detecting enough bands
  - *Typically, 7 - 9 bands are required for good indexing.*
- Accurate band direction determination
  - *Orientation determination uses the angles between the bands. When the determined angle is outside the measurement tolerance (typically 3° - 5°), indexing may fail.*
- Minimal pattern shadowing
  - *Surface topography may produce shadows on the EBSD detector that can be interpreted as bands, causing indexing to fail.*

These requirements effectively limit EBSD analyses to materials that are flat, produce good EBSD patterns, and are not too heavily deformed. Materials that produce only very weak patterns, are beam sensitive, or have severe damage to the crystal lattice causing significant blurring of the EBSD patterns, have always been difficult to analyse and alternative methods are normally used for their characterisation.

The main reason for indexing problems is when the position and direction of the EBSD bands in the patterns has becomes too difficult to determine. There is also a greater probability of merging information from adjacent grains or sub-grains into overlapping patterns in fine-grained and deformed materials, which complicates the indexing. A typical example of EBSD mapping limitations using Hough-based band detection is shown in the map in Fig. 12. This is a cross-section EBSD map of a deformed Ti-alloy where a surface treatment caused additional severe deformation at the upper edge of the sample. In the interior of the material the patterns are already weak, but in most patterns enough bands can be identified for successful indexing. The additional damage to the crystal lattice near the surface makes the diffracted signal in the EBSD patterns so faint that band detection and indexing fails as indicated by the random colour speckling.

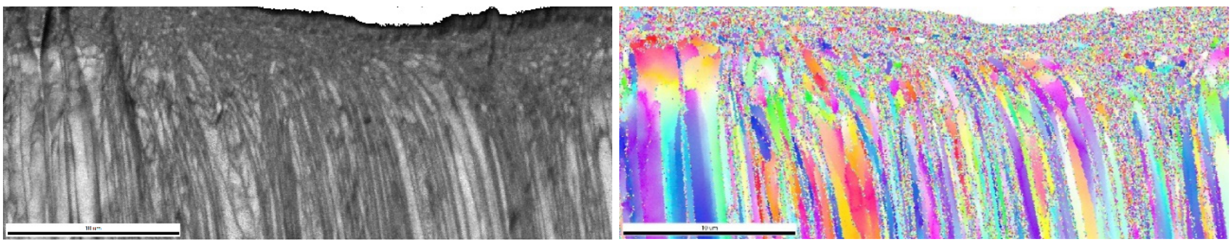

Figure 12. EBSD map of Ti-alloy with severe surface deformation measured using Hough-based indexing.

5. *SPHERICAL INDEXING*

An alternative indexing method has been developed that does not rely on the detection of the individual bands, but instead uses the entire pattern image to determine the orientation, spherical indexing [1]. During off-line reprocessing the recorded experimental EBSD patterns are matched against a dynamic simulation of all possible orientations contained in a master pattern. Such a master pattern is generated by simulating the diffraction paths of up to 2 billion electrons in all directions through a crystal using a Monte Carlo model [2]. The crystal model contains an accurate description of the lattice parameters and atomic positions for a specific phase. The intensities of the diffracted electrons are then captured on a sphere surrounding this crystal to cover all possible direction (Figs. 13 and 14).

Figure 13. Simulated diffraction intensities on a spherical master pattern.

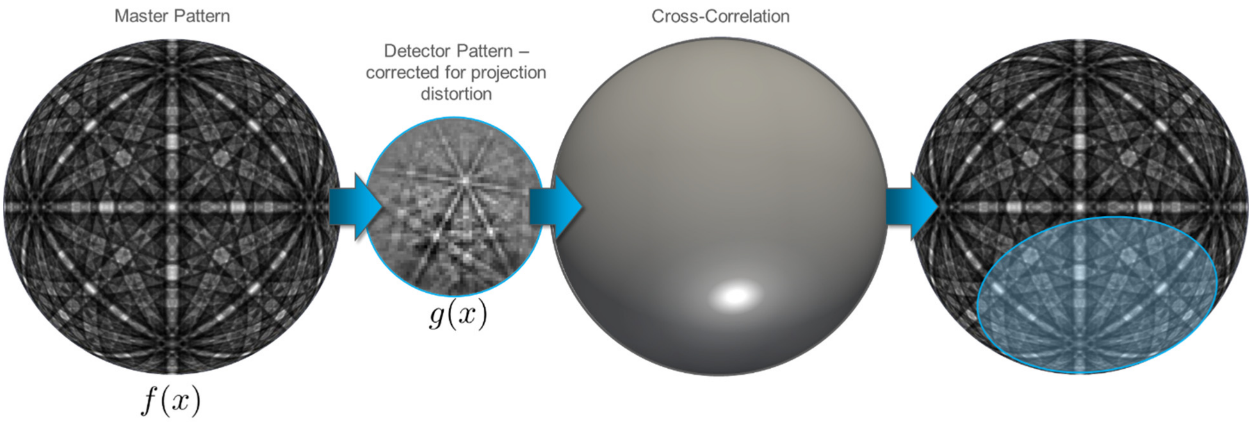

Figure 14. Spherical indexing procedure: The experimental EBSD patterns are "projected" onto the surface of the simulated sphere and a cross-correlation for all possible positions on.

Because the entire pattern is used, the spherical indexing method is extremely sensitive to small differences in EBSD patterns. This allows successful discrimination of pseudosymmetric orientations and most crystallographic point groups. As there is no need to accurately detect a minimum number of individual bands, the method is also extremely sensitive to extract diffraction information in poor quality EBSD patterns. Fragmented information of bands in combination with zone axes (band intersections which are typically brighter than the background) is enough. The indexing improvement is illustrated with the reprocessed deformed Ti-alloy from Fig. 12 (Fig. 15).

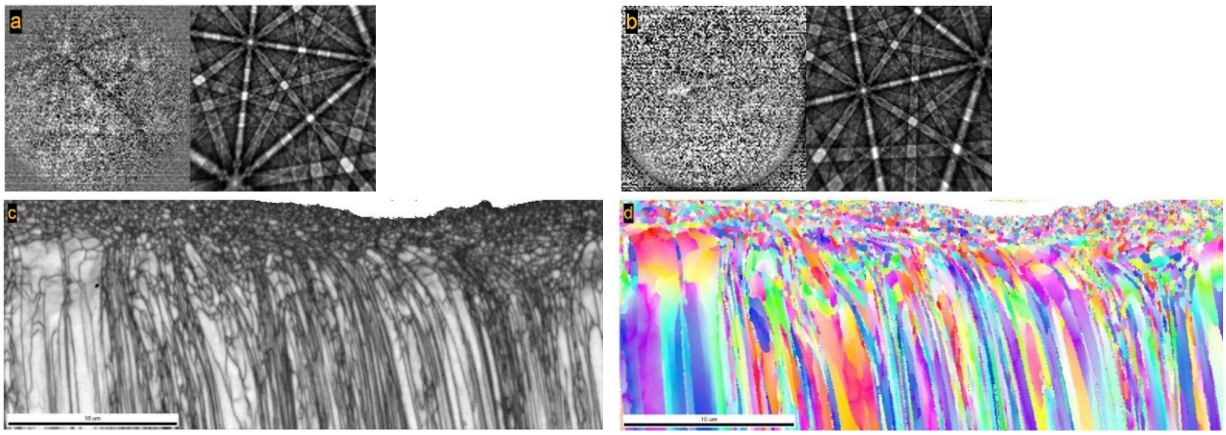

Figure 15. EBSD map of Ti-alloy with severe surface deformation after off-line spherical indexing reprocessing. a) EBSD pattern from the substrate with simulation; b) EBSD pattern from the deformed surface area simulation; c) Cross-correlation map illustrating the fit between the patterns and the simulation; d) IPF map.

Moreover, spherical indexing improves the orientation precision of the EBSD measurements. In conventional Hough transform-based indexing, small errors in the detection of the individual bands affect the overall orientation determination, which can be avoided using full pattern matching. Similarly, overlapping patterns at grain boundaries can be indexed with the same precision as single patterns inside grains as only one of the overlapping patterns gets fitted to the Spherical Indexing master pattern. This results in higher orientation precision at grain boundaries, which for example improves sharpness in KAM maps (Fig. 16).

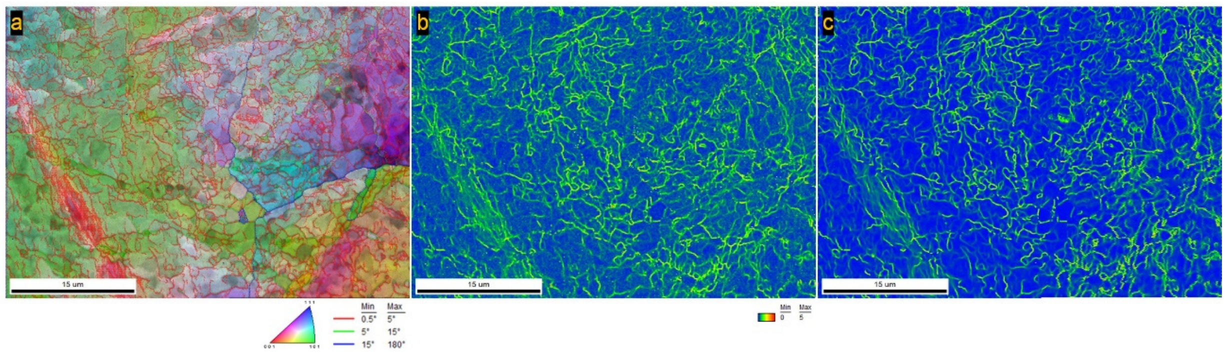

Figure 16. EBSD map of deformed Pt. a) IPF map with grain boundaries; b) Kernel average misorientation (KAM) map by triplet voting (Hough-based) indexing; c) KAM map with improved precision after spherical indexing.

6. NEIGHBOUR PATTERN AVERAGING AND REINDEXING (NPAR)

When the pattern quality is extremely poor or when the analysis surface is not planar and shadowing occurs in the EBSD patterns from surface topography, an additional image processing step may be applied. The neighbour pattern averaging and reindexing (NPAR) method optimises the signal to noise ratio in EBSD patterns by averaging each pattern with a ring of patterns around it (Fig. 17) [3].

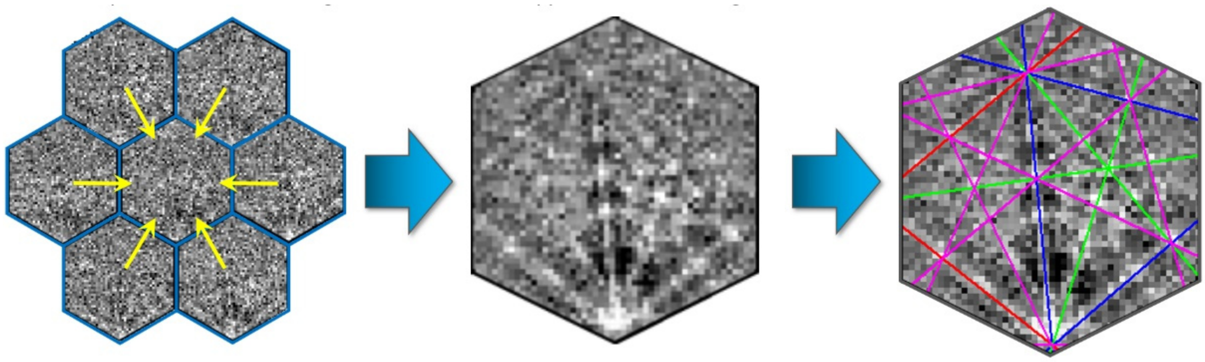

Figure 17. NPAR procedure. Each pattern is averaged with a ring of neighbours before indexing.

Random noise will then get smoothed out and weak bands will become more visible. Additionally, any shadow edges caused by topography will change slightly between the patterns and become less pronounced in the averaged pattern (Fig. 18).

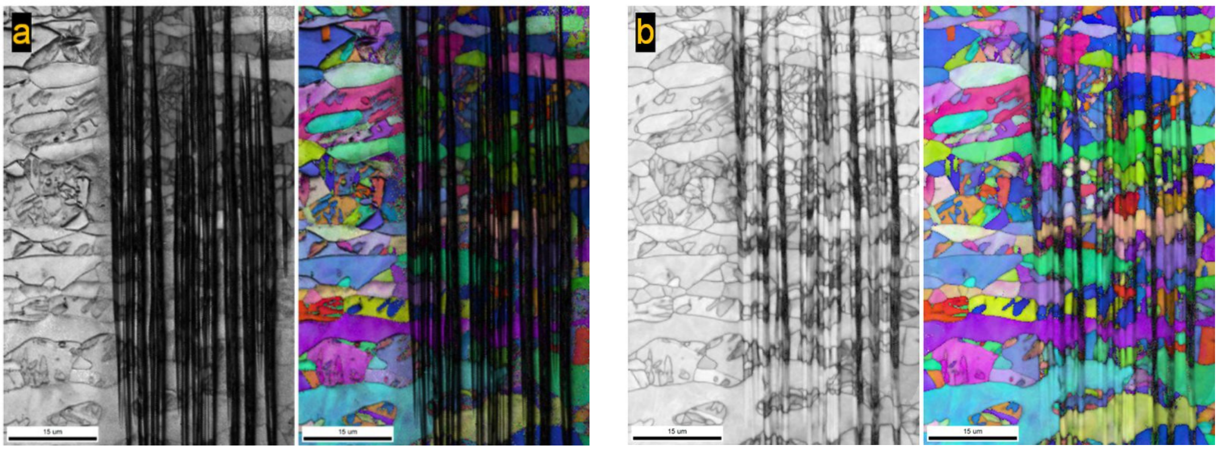

Figure 18. NPAR Indexing improvement. a) Specimen with strong topography and locally poor indexing due to shadowing of the EBSD patterns. b) Patterns in shadowed areas on the sample surface have been recovered and allow successful indexing.

The combination of direct detection, NPAR, and spherical indexing provides the maximum extension of the capabilities of EBSD mapping. This increases the sensitivity gains and fully utilises the improved pattern quality of the direct detection EBSD patterns. The sensitivity gains are especially useful for beam sensitive samples like (semi-)organic perovskites or biominerals (Fig. 19). In some cases, collecting a single SEM image already damages the crystal structure to such an extent that no patterns can be generated afterwards. Increasing the exposure time or the beam current will only cause more damage and only EBSD mapping at low kV and low current (e.g., 6 kV and 100 pA) allows collection of weak patterns, which can then be analysed with spherical indexing together with NPAR.

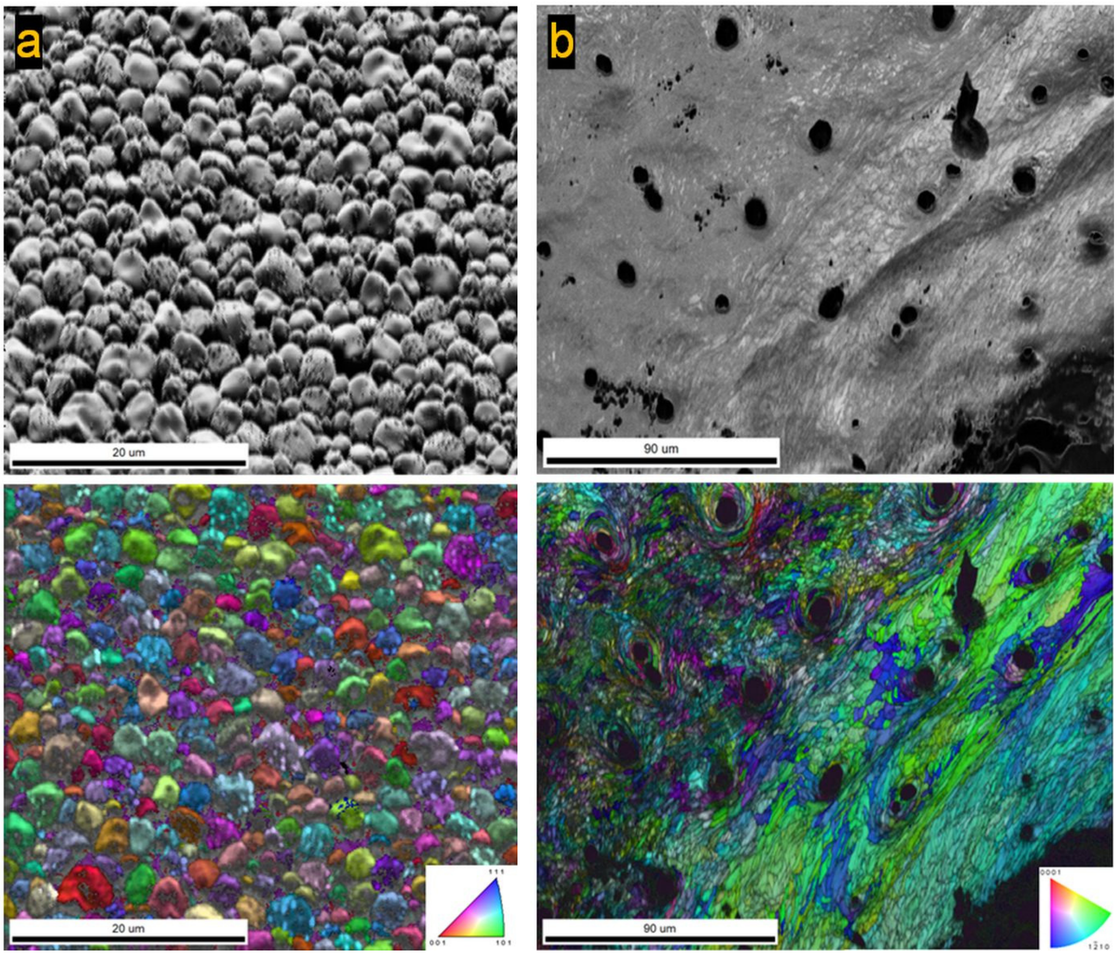

Figure 19. EBSD maps on beam sensitive materials using direct detection and NPAR. a) $MAPbI_3$ perovskite; b) Brachiopod shell.

7. CONCLUSIONS

Direct detection of EBSD patterns and the introduction of spherical indexing have extended the range of materials that can be successfully characterised with electron backscatter diffraction. The absence of a phosphor screen and lens system allows for collection of distortion-free diffraction patterns enabling quantitative pattern analysis. Indexable patterns can be obtained with fewer than 10 electrons per pixel allowing for successful analysis of beam sensitive materials at minimal beam energies and currents. This also improves lateral resolution for regular EBSD mapping.

Spherical indexing is an alternative method to Hough-based indexing that uses full pattern matching to dynamic simulations instead of individual band detection. Spherical indexing enables orientation determination directly up to the grain boundaries with improved lateral resolution and improved orientation precision. Extremely weak and noisy patterns can be successfully indexed in highly deformed and beam sensitive materials as the full pattern matching enables the use of fragmented patterns and severe pattern overlaps. Combining direct detection and spherical indexing with NPAR expands the application of EBSD even further to materials that could not be analysed before.

8. REFERENCES

[1] Lenthe W, Singh S and De Graef M 2019 *Ultramicroscopy* **207** 112841
[2] Callahan P G and De Graef M 2013 *Microsc. Microanal.* **19** 1255-1265
[3] Wright S I, *et al.* 2015 *Ultramicroscopy* **159** 81-94